

Anisotropic surface transport in topological insulators in proximity to a helical spin density wave

Qiuzi Li,¹ Parag Ghosh,² Jay D. Sau,¹ Sumanta Tewari,³ and S. Das Sarma¹

¹*Condensed Matter Theory Center and Joint Quantum Institute, Department of Physics, University of Maryland, College Park, Maryland, 20742-4111, USA*

²*Department of Physics and Astronomy, George Mason University, Fairfax, Virginia, 22030, USA and 100 Bureau Drive, Stop 8410, NIST, Gaithersburg, Maryland, 20899-8410, USA*

³*Department of Physics and Astronomy, Clemson University, Clemson, South Carolina, 29634, USA*
(Dated: February 10, 2019)

We study the effects of spatially localized breakdown of time reversal symmetry on the surface of a topological insulator (TI) due to proximity to a helical spin density wave (HSDW). The HSDW acts like an externally applied one-dimensional periodic(magnetic) potential for the spins on the surface of the TI, rendering the Dirac cone on the TI surface highly anisotropic. The decrease of group velocity along the direction \hat{x} of the applied spin potential is twice as much as that perpendicular to \hat{x} . At the Brillouin zone boundaries (BZB) it also gives rise to new semi-Dirac points which have linear dispersion along \hat{x} but quadratic dispersion perpendicular to \hat{x} . The group velocity of electrons at these new semi-Dirac points is also shown to be highly anisotropic. Experiments using TI systems on multiferroic substrates should realize our predictions.

PACS numbers: 71.10.Pm, 73.20.-r

In the last few years there has been a growing interest in topological insulators (TI), which are materials that are insulators in the bulk but conduct two-dimensionally on the surfaces [1–6]. The non-trivial topology of the wavefunction of such TI has been predicted to show metallic surface conductivity that is topologically protected against weak disorder and interaction effects. One of the mechanisms by which the surface modes can be disrupted is by breaking the time reversal invariance upon applying a magnetic field. There have been several studies on the effects of a magnetic field either applied directly perpendicular to the surface of a TI [7] or by the proximity effect of a ferromagnet in a heterostructure [8, 9]. On the other hand, the effects of an antiferromagnet or a spin density wave on the surface states of the TI is a topic which is much less well-explored. We carry out such an analysis of the effect of a spin density wave on TI transport in this work.

Although an antiferromagnet, in the proximity to a TI, does not affect the global time reversal symmetry (TRS) in the latter, the staggered nature of the spins in the antiferromagnet breaks the TRS locally. In this work, we are interested in how this local TRS breaking affects the surface states of the TI. However, the local TRS breaking occurs at a length scale which is of the order of the lattice spacing in the antiferromagnet (for e.g., 8.85\AA for MnO). Therefore the effects of local TRS breaking occur at very large momenta, which makes it difficult to observe them in experiments. In order to redress this difficulty, we propose to study the effects of local TRS breaking by replacing the antiferromagnet with a multiferroic material [10] like orthorhombic RMnO₃ (R being a rare earth element like Tb or Dy) or the family of Fe_{1-x}Co_xSi with cubic but noncentrosymmetric structure, which shows a heli-

cal spin density wave (HSDW) order with relatively long periods ($> 30\text{nm}$) [11]. The HSDW acts like an externally applied potential for the spins on the surface of the topological insulator. The situation is similar to that of an externally applied charge potential on graphene [12]. However, the contrast between the two situations is that the 3D topological insulator has spin polarized 2D Dirac fermions on its surface [13], whereas the Dirac fermions in graphene carry pseudo-spin. Nevertheless, in analogy with the charge potential applied to graphene, a spin potential can be used for TI to manipulate the surface Dirac fermions.

We find that the surface states of the TI are significantly modified in the presence of the HSDW. The HSDW acts like an externally applied superlattice potential on the TI surface resulting in striking anisotropy of the Dirac cones and group velocity of the surface states. In particular, the group velocity along the direction of the superlattice is monotonically suppressed as a function of the lattice potential strength and its period. For the type of HSDW considered in this paper, which we call proper HSDW, [14] (see below), we find that novel semi-Dirac points, whose low-energy characteristics are intermediate between Dirac (massless) and zero-gap (massive) semiconductors [15, 16], show up on the BZB.

We begin by writing down the effective Hamiltonian for the low-energy quasiparticles on the surface of a topological insulator as,

$$H_0(\mathbf{k}) = \hbar v_F (k_x \sigma_x + k_y \sigma_y) \quad (1)$$

where $v_F \simeq 6.2 \times 10^5 \text{m/s}$ is the Fermi velocity of Dirac fermions in Bi₂Se₃ [17] and σ_i are the Pauli matrices. The Hamiltonian in Eq. (1) is characterized by an energy spectrum $\varepsilon_{s,k} = s \hbar v_F k$ where $s = \pm 1$ is the band index,

and eigenstates given by

$$\langle \mathbf{r} | s, \mathbf{k} \rangle = \frac{1}{\sqrt{2}} e^{i\mathbf{k} \cdot \mathbf{r}} \begin{pmatrix} 1 \\ s e^{i\theta_{\mathbf{k}}} \end{pmatrix}, \quad (2)$$

where $\theta_{\mathbf{k}}$ is the angle of vector \mathbf{k} with respect to the \hat{k}_x direction.

In the presence of the HSDW on top of a TI, depicted schematically in Fig. 1, the Hamiltonian (1) is modified [18] to: $H = H_0(\mathbf{k}) + U(x)$, where the potential $U(x)$ for the HSDW can be written as:

$$U(x) = U_y \sigma_y \cos\left(\frac{2\pi}{L}x\right) + U_z \sigma_z \sin\left(\frac{2\pi}{L}x\right), \quad (3)$$

where L is the spatial period of the potential, and $U_{y,z}$ are the amplitudes of the HSDW [14]. For the case $U_z < U_y$, we find no gapless states on the BZB. On the other hand, for $U_z > U_y$, two Dirac points centered at $(\frac{\pi}{L}, \pm K_y)$ emerge on the BZB. For the symmetric HSDW such that $U_z = U_y = U_0$, which we shall call proper HSDW, we find a single semi-Dirac point at $(k_x, k_y) = (\pm \frac{\pi}{L}, 0)$ (Fig. 1c). In this work, we shall focus on the case of a proper HSDW on TI.

The exchange-induced potential $U(x)$ from the HSDW creates a periodic potential on the surface of the TI. The electronic eigenstates of such a Hamiltonian can be written using Bloch's theorem as

$$\psi_{n\mathbf{k}}(\mathbf{r}) = \sum_{\mathbf{G}} e^{i(\mathbf{k}+\mathbf{G}) \cdot \mathbf{r}} c(n, \mathbf{k} + \mathbf{G}) \quad (4)$$

where $\mathbf{G} = \frac{2m\pi}{L} \hat{x}$ ($m \in \text{integer}$) is the reciprocal lattice vector, $\psi_{n\mathbf{k}}(\mathbf{r})$ and $c(n, \mathbf{k} + \mathbf{G})$ are 2-spinor functions and n is the band-index. Here k_x is only limited to be in the first Brillouin Zone (FBZ), i.e. $k_x \in [-\frac{\pi}{L}, \frac{\pi}{L}]$. The band eigenstates $\psi_{n\mathbf{k}}(\mathbf{r})$ and the corresponding eigen-energies $E_n(\mathbf{k})$ are obtained as eigenvalues and eigenvectors of the Bloch equation

$$\begin{aligned} & [\hbar v_F ((k_x + G)\sigma_x + k_y\sigma_y) - E_{n\mathbf{k}}] c(n, \mathbf{k} + \mathbf{G}) \\ & + (U_y \sigma_y + iU_z \sigma_z) \frac{c(n, \mathbf{k} + \mathbf{G} - \frac{2\pi}{L})}{2} \\ & + (U_y \sigma_y - iU_z \sigma_z) \frac{c(n, \mathbf{k} + \mathbf{G} + \frac{2\pi}{L})}{2} = 0. \end{aligned} \quad (5)$$

While the above Bloch equation may be solved by numerical diagonalization to obtain numerical eigenvalues and eigenvectors, more insight can be obtained into the solutions around high symmetry points in the FBZ at $\mathbf{k} = 0$ and at the BZB by using perturbation theory. The numerical results of diagonalizing Eq. 5 are shown in Fig. 2, Fig. 3 and Fig. 4. The total Hamiltonian $H_0 + U$ of the TI+HSDW system is invariant under a composite

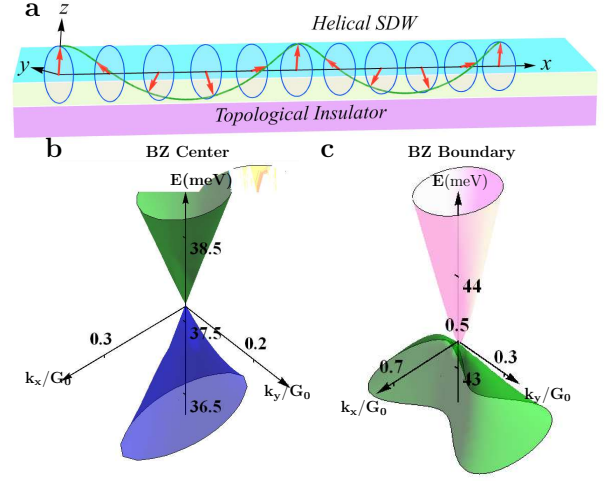


FIG. 1: (Color online) (a) Schematic diagram of the system. The HSDW is on top of the topological insulator with the periodicity L . (b) Energy of charge carriers with $U_0 = 0.05$ eV, $L = 90$ nm for the first band above (green) and below (blue) the original Dirac cone versus 2D wavevector \mathbf{k} . (c) Energy of charge carriers for the first (green) and the second (Pink) band near the semi-Dirac Point on BZB being zoomed in near $(k_x, k_y) = (\frac{\pi}{L}, 0)$.

symmetry $S = \Theta T$ where Θ is the time-reversal operator and T is the operator corresponding to translation by $L/2$. Since, the operator S , similar to the time-reversal symmetry operator Θ , is both anti-unitary and satisfies $S^2 = -1$, the proximity to the HSDW does not open a gap at $\mathbf{k} = 0$. In other words, the HSDW preserves the global time-reversal symmetry, it does not open up a gap near $\mathbf{k} = 0$ on the TI surface.

In the limit of a perturbatively weak coupling to the HSDW ($\frac{|U(\mathbf{G})|}{\hbar v_F |\mathbf{G}|} \ll 1$), the leading order contribution of the HSDW to the low-momentum ($\mathbf{k} \sim 0$) dispersion can be characterized by the renormalization of the group velocity and effective mass at $\mathbf{k} = 0$. The group velocity of states without the HSDW is isotropic around $\mathbf{k} = 0$ with constant magnitude v_F . In presence of the HSDW, the renormalized group velocity of quasiparticles parallel to the wavevector \mathbf{k} [$v_{\hat{k}} \equiv \mathbf{v}(\mathbf{k}) \cdot \hat{k}$] around the Dirac point ($|k| \ll 1$) obtained within second order perturbation theory can be written as

$$\frac{v_{\hat{k}} - v_F}{v_F} = \frac{1}{\hbar v_F} \frac{\partial(E_{+,k} - \varepsilon_{+,k})}{\partial k} = -\frac{U_0^2 L^2}{8\pi^2 \hbar^2 v_F^2} (3 + \cos 2\theta_{\mathbf{k}}) \quad (6)$$

From Eq. (6), it is clear that the renormalized group velocity is anisotropic around the Dirac point and decays monotonically both with the amplitude of periodic potential U_0 and spatial period L of the potential. Fig. 2 shows the result from a full numerical calculation. We note that there is good agreement between the trends from Eq. (6) and the full calculation (shown in Fig. 2a)

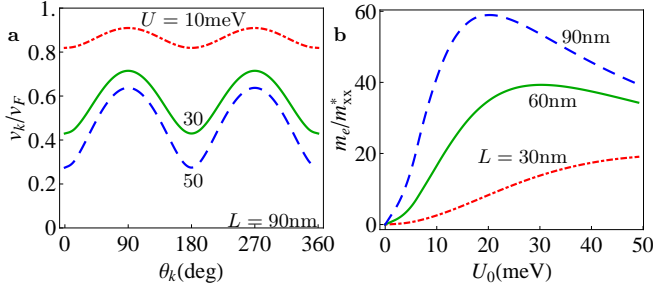


FIG. 2: (Color online) (a) The group velocity v_k (measured from the Dirac point) of charge carriers on the surface of the TI in units of the Fermi velocity (v_F) versus the angle θ_k with $L = 90\text{nm}$. Dotted red, solid green and dashed blue lines correspond to U_0 being 10 meV, 30 meV and 50 meV, respectively. (b) The inverse effective mass m_e/m_{xx}^* versus U_0 for the first band above the Dirac point on BZ center. Dotted red, solid green and dashed blue lines are results for L being 30nm, 60nm and 90nm, respectively.

for weak potential strength.

The interaction with the HSDW introduces a finite curvature along the x -direction to the previously linear in \mathbf{k} dispersion of the Dirac fermions at $\mathbf{k} \sim 0$. The effective mass tensor at $\mathbf{k} = 0$ from the curvature of the energy band around the Dirac point is given by

$$\left(\frac{m_e}{m^*}\right)_{\alpha\beta} = \frac{m_e}{\hbar^2} \frac{\partial^2 E(\mathbf{k})}{\partial k_\alpha \partial k_\beta} \Big|_{\mathbf{k}=0} = \begin{cases} 0, & \alpha, \beta = y, \text{ or } \alpha \neq \beta \\ \frac{8U_0^2 m_e}{\hbar^3 v_F G_0^3}, & \alpha, \beta = x \end{cases} \quad (7)$$

where m_e is the bare electron mass and $G_0 = \frac{2\pi}{L}$. From Eq. (7) the effective mass m_e/m_{xx}^* grows as U_0^2 , which describes the small U_0 behavior of the numerically determined effective mass shown in Fig. 2b.

While the periodic potential from the HSDW introduced renormalizations of the velocity and effective masses at the center of the Dirac cone at $\mathbf{k} = 0$, the effect of the periodic potential was limited to being perturbative since there was no degeneracy in the initial Dirac spectrum near $\mathbf{k} = 0$ that was directly connected by the potential U . However, such degeneracies do occur at the edges of the FBZ, which we have referred to as the BZB, and non-perturbative effects of the potential may be generated by coherent back scattering with momenta \mathbf{G} . Unlike the case of conventional crystals, where such back-scattering opens up gaps, one finds the emergence of new Dirac cones at the BZB in the presence of interaction with the HSDW (Fig. 3a).

When the wavevector \mathbf{k} is on the first BZB ($(k_x, k_y) = (\pi/L, k_y)$), the two states $|s, \mathbf{k}\rangle$ and $|s, \mathbf{k} - (2\pi/L, 0)\rangle$ are degenerate before the periodic potential is applied. In the presence of an applied potential, the largest contribution to the energy eigenvalues at the edges of the BZ comes

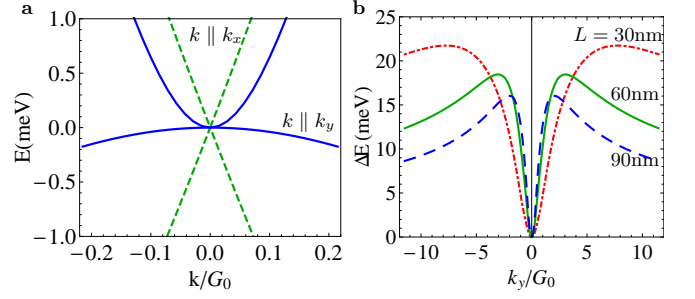


FIG. 3: (Color online) (a) Semi-Dirac charge carrier dispersion versus the wavevector \mathbf{k} with \mathbf{k} measured from $(k_x, k_y) = (\frac{\pi}{L}, 0)$ on the BZB. Dashed (green) and solid (blue) lines show the linear dispersion along the x direction and the quadratic dispersion along the y direction, respectively with $U_0 = 50\text{meV}$ and $L = 90\text{nm}$ ($E(\pi/L, 0)$ was shifted to zero). (b) The energy gap ΔE between the first and the second band at the BZB versus k_y for charge carriers above the Dirac point with $U_0 = 50\text{meV}$. Dotted red, solid green and dashed blue lines correspond to L being 30 nm, 60 nm and 90 nm, respectively.

from these two degenerate states. For the clockwise helix, the backscattering amplitude leads to an energy gap on the BZB that is given by,

$$\Delta E(k_y) = U_0 \left(1 - \frac{s}{\sqrt{1 + (k_y L/\pi)^2}} \right), \quad (8)$$

where $s = \pm 1$ represents the positive or negative bands in the Dirac cone. In the lower band of the Dirac cone, i.e. $s = -1$, the above gap is maximum at $k_y = 0$ and decreases monotonically with $|k_y|$. The positive band is more interesting with a gap that vanishes at $k_y = 0$, and increases monotonically then decreases with $|k_y|$ as seen in (Fig. 3b). The maximum gap opening is proportional to the amplitude of the external potential in the weak potential regime.

As with the Dirac cone at $\mathbf{k} = 0$, an understanding of the low-energy dispersion and the corresponding transport properties associated with the Dirac cone at the BZB is obtained by calculating the group velocity and effective mass. Second order perturbation theory leads to a strongly anisotropic group-velocity v_k measured from the gap-less point at $(k_x, k_y) = (\frac{\pi}{L}, 0)$ which is written as

$$v_k = \frac{\hbar v_F^2 G_0 \cos \theta_k}{\sqrt{U_0^2 + \hbar^2 v_F^2 G_0^2}} \quad (9)$$

For comparison, the full numerical calculation is shown in Fig. 4. The effective mass tensor at the new gapless point, calculated within second order perturbation theory

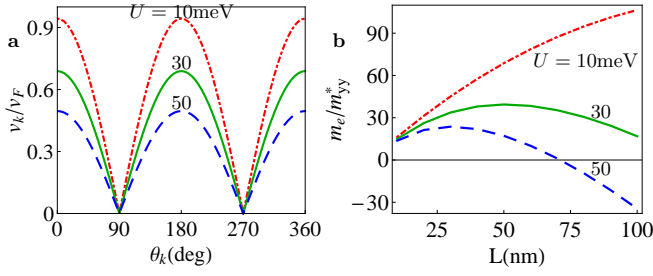


FIG. 4: (Color online) (a) Anisotropic v_k/v_F measured from the semi-Dirac point on the BZB versus the angle θ_k with $L = 90$ nm. Dotted (red), solid (green) and dashed (blue) lines correspond to U_0 being 10 meV, 30 meV and 50 meV, respectively. (b) The inverse effective mass m_e/m_y^* versus L around the point $(k_x, k_y) = (\frac{\pi}{L}, 0)$ for the lower band of the semi-Dirac point for three U_0 . Note the negative effective mass (corresponding to Fig. 3 (a)).

similar to Eq. 7, is given by

$$\left(\frac{m_e}{m^*}\right)_{\alpha\beta} \Big|_{\mathbf{k}=(\pi/L,0)} = \begin{cases} 0, & \alpha, \beta = x, \text{ or } \alpha \neq \beta \\ 2(\hbar v_F G_0 \pm U_0)/G_0^2, & \alpha, \beta = y \end{cases} \quad (10)$$

where the \pm corresponds to the upper or lower band around the semi-Dirac point at $(k_x, k_y) = (\frac{\pi}{L}, 0)$. Eq. 9 and 10 together show the highly anisotropic dispersion of the semi-Dirac point on BZB: a dispersion linear along the periodic direction \hat{x} but quadratic along the perpendicular direction \hat{y} . Fig. 4a shows the angular dependence of the group velocity $v_{\mathbf{k}}$ from a full numerical calculation. The velocity v_y is seen to have zero component regardless of the strength of the applied potential. The dependence of the renormalized group velocity v_k/v_F is a decreasing function of the amplitude of the applied potential. In Fig. 4b, we plot the dependence of the inverse effective mass of the lower-band of the semi-Dirac point at the BZB (in the vicinity of $(k_x, k_y) = (\frac{\pi}{L}, 0)$) on the applied potential period L and amplitude U_0 respectively. We find that the effective mass along the y -direction changes sign from positive to negative as a function of L and U_0 . The dispersion at small k_y for parameters U, L_0 corresponding to negative effective mass is shown in Fig. 3(a). In this case, the bands at larger k_y turn up leading to the emergence of another fermi surface. There is no such fermi surface doubling for parameters with positive mass.

In summary, we have considered the effects of a helical spin density wave on the surface states of a topological insulator. We find that the HSDW acts like an effective spin potential on the TI surface and breaks the local time reversal invariance in the latter. The applied spin potential has two main consequences: First, the group velocity of electrons at the Dirac point is strongly suppressed in the direction transverse to the periodic potential. Sec-

ondly, new semi-Dirac points emerge for the first upper (lower) band at the Brillouin zone boundaries that corresponds to the right-handed (left-handed) chirality of the applied HSDW. The semi-Dirac points are characterized by linear dispersion parallel to the direction \hat{x} of the applied periodic potential but quadratic dispersion perpendicular to the \hat{x} direction. When the chemical potential of the TI is such that the semi-Dirac points at the BZBs give the main contribution to transport, we expect the surface transport properties to be highly anisotropic. This is because at these points, the dispersion is linear in one direction and quadratic in the other. The momentum space location of these new semi-Dirac cones can also be manipulated by applying an in-plane magnetic field to the HSDW. Such a magnetic field [10] can change the orientation of the spin rotation axis relative to the pitch vector of the HSDW. By studying the effects of such a change in the applied periodic potential on the new semi-Dirac cones it should be possible to isolate the surface state contribution from the bulk in the total conductance in topological insulators with relatively small bulk gaps. One particular advantage of our proposal is that the proposed experiment can be carried out in the existing TI systems without any problem arising from the bulk conduction which is invariably present in all current TI systems since the bulk transport is presumably unaffected by the presence of the HSDW.

Q.L. acknowledges helpful discussions with Kai Sun. Q.L., J.D.S. and S.D.S. are supported by DARPA-QuEST, JQI-NSF-PFC. P.G. is supported by National Institute of Standards and Technology through Grant Number 70NANB7H6138, Am 001 and through Grant Number N000-14-09-1-1025A by the Office of Naval Research. S.T. acknowledges support from AFOSR and Clemson University start up funds.

-
- [1] X. Qi, T. Hughes, and S. Zhang, *Physical Review B* **78**, 195424 (2008).
 - [2] D. Hsieh, Y. Xia, L. Wray, D. Qian, A. Pal, J. Dil, J. Osterwalder, F. Meier, G. Bihlmayer, C. L. Kane, et al., *Science* **323**, 919 (2009).
 - [3] H. Zhang, C. Liu, X. Qi, X. Dai, Z. Fang, and S. Zhang, *Nature Physics* **5**, 438 (2009).
 - [4] R. Roy, *Physical Review B* **79**, 195322 (2009).
 - [5] Y. Chen, J. Analytis, J. Chu, Z. Liu, S. Mo, X. Qi, H. Zhang, D. Lu, X. Dai, Z. Fang, et al., *Science* **325**, 178 (2009).
 - [6] M. Z. Hasan and K. C. L., arXiv:1002.3895 and references therein.
 - [7] W.-K. Tse and A. H. MacDonald, *Phys. Rev. Lett.* **105**, 057401 (2010).
 - [8] S. Mondal, D. Sen, K. Sengupta, and R. Shankar, *Phys. Rev. Lett.* **104**, 46403 (2010).
 - [9] I. Garate and M. Franz, *Phys. Rev. Lett.* **104**, 146802 (2010).

- [10] S.-W. Cheong and M. Mostovoy, *Nature Materials* **6**, 13 (2007).
- [11] M. Uchida, Y. Onose, Y. Matsui, and Y. Tokura, *Science* **311**, 359 (2006).
- [12] C.-H. Park, L. Yang, Y.-W. Son, M. L. Cohen, and S. G. Louie, *Nature Phys.* **4**, 213 (2008).
- [13] Y. Xia, D. Qian, D. Hsieh, L. Wray, A. Pal, H. Lin, A. Bansil, D. Grauer, Y. S. Hor, R. J. Cava, et al., *Nature Phys.* **5**, 398 (2009).
- [14] H. spin density wave due to antisymmetric exchange interaction, *J. Phys. Soc. Jpn.* **50**, 3888 (1981).
- [15] S. Banerjee, R. R. P. Singh, V. Pardo, and W. E. Pickett, *Phys. Rev. Lett.* **103**, 016402 (2009).
- [16] V. Pardo and W. E. Pickett, *Phys. Rev. Lett.* **102**, 166803 (2009).
- [17] H. Zhang, C.-X. Liu, X.-L. Qi, X. Dai, Z. Fang, and S.-C. Zhang, *Nature Phys.* **5**, 438 (2009).
- [18] T. Yokoyama, Y. Tanaka, and N. Nagaosa, *Phys. Rev. B* **81**, 121401(R) (2010).